

Investigations on a vortex induced vibration based energy harvester

S. Krishna Kumar, Chandan Bose, Shaikh Faruque Ali, Sunetra Sarkar, and Sayan Gupta

Citation: [Appl. Phys. Lett.](#) **111**, 243903 (2017);

View online: <https://doi.org/10.1063/1.5001863>

View Table of Contents: <http://aip.scitation.org/toc/apl/111/24>

Published by the [American Institute of Physics](#)

Articles you may be interested in

[Design of multi-frequency acoustic kinoforms](#)

Applied Physics Letters **111**, 244101 (2017); 10.1063/1.5004040

[Fractional memristor](#)

Applied Physics Letters **111**, 243502 (2017); 10.1063/1.5000919

[Sustaining high-energy orbits of bi-stable energy harvesters by attractor selection](#)

Applied Physics Letters **111**, 213901 (2017); 10.1063/1.5000500

[Improved perovskite morphology and crystallinity using porous \$\text{PbI}_2\$ layers for efficient planar heterojunction solar cells](#)

Applied Physics Letters **111**, 243902 (2017); 10.1063/1.5012135

[Phase retrieval of an electron vortex beam using diffraction holography](#)

Applied Physics Letters **111**, 223101 (2017); 10.1063/1.4998595

[Study for optimizing the design of optical temperature sensor](#)

Applied Physics Letters **111**, 241905 (2017); 10.1063/1.5010698

Scilight

Sharp, quick summaries **illuminating**
the latest physics research

Sign up for **FREE!**

AIP
Publishing

Investigations on a vortex induced vibration based energy harvester

S. Krishna Kumar,¹ Chandan Bose,¹ Shaikh Faruque Ali,¹ Sunetra Sarkar,²
 and Sayan Gupta¹

¹Department of Applied Mechanics, Indian Institute of Technology Madras, Chennai 600036, India

²Department of Aerospace Engineering, Indian Institute of Technology Madras, Chennai 600036, India

(Received 28 August 2017; accepted 1 December 2017; published online 14 December 2017)

This study investigates energy harvesting from vortex induced vibrations of a flexible cantilevered flapper placed in the wake of a rigid circular cylinder. The effect of the gap between the cylinder and the flapper on the energy harvested is investigated through wind tunnel experiments and numerical simulations. As the flow speed is varied, a transition in the flapper dynamics is observed, which in turn affects the power extracted by the harvester. Numerical investigations reveal that the flapper dynamics is different depending on whether the vortices are shed ahead or behind the flapper. This study concludes that the choice of the gap influences the energy harvesting potential of such harvesters. *Published by AIP Publishing.* <https://doi.org/10.1063/1.5001863>

Devices that harvest energy based on flow induced vibrations can be broadly classified into either flutter based or vortex induced vibration (VIV) based energy harvesters.^{1,2} The former category essentially involves a streamlined body, such as an airfoil or a plate, behaves as a coupled fluid-structure interaction (FSI) system, and undergoes sustained oscillations when the flow speed is above a critical velocity. The trigger for flutter oscillations comes from mechanical perturbation or movement of the body, which in turn generates aerodynamic loads. Beyond a critical wind speed, these loads are strong enough to sustain the oscillation. Hence, it is also called a movement induced (FSI) excitation (MIE).³ In classical pitch-plunge airfoil based harvesters, flow induced oscillations (and hence harvesting of energy) occur only beyond a critical wind speed.⁴ However, energy harvesting is possible even at lower speeds by providing actuation mechanisms along, say the torsional mode, that increases the aerodynamic lift which in turn enhance the bending movement. In the aeroelastic literature, this is known as aerodynamic coupling. Thus, with the help of external actuation force and through aerodynamic coupling, combined bending-torsion oscillation can be achieved even below the critical wind speed.⁵ In flutter based harvesters, the use of a streamlined body such as an airfoil or a plate is crucial in order to generate the necessary aerodynamic loads. Comprehensive reviews on flutter based energy harvesters are available in the literature.^{6–8}

On the other hand, VIV is the result of flow instabilities behind bluff bodies. A bluff body, by the virtue of its shape, releases a von Kármán wake behind it. The wake with its repetitive structure can induce oscillations in the bluff body itself if it is free to move. As opposed to MIE systems (like flutter), vortex induced vibration of bluff bodies comes under instability induced (FSI) excitation (IIE). However, a wake can also impart input fluctuations to a flexible structure kept at the downstream of the bluff body. When the wake induces oscillation to the downstream structure, essentially behaving like an external source of oscillation to the structure, it is a case of externally induced (FSI) excitation (EIE).³ The harvester proposed in this study belongs to the second kind of VIV based systems.

These type of VIV based smart energy harvesters usually consist of a rigidly fixed bluff body upstream of a thin flexible plate like structure called the flapper.^{9–11} These flappers are typically made of smart materials—usually piezoelectric materials which develop an electric potential under mechanical strains. The vortices generated by the flow due to the presence of the bluff body induce time varying forces on the flapper causing it to vibrate, which in turn leads to the development of an electric potential that can be harvested as electrical energy.^{1,7,8} The harvester being considered in this study belongs to this genre.

In the absence of any downstream structures, the vortex shedding past a bluff body—typically taken to be a cylinder—depends on the Reynolds number (Re).¹² The presence of downstream structures—such as the flappers—leads to variations in the wake structures, modifying the shedding frequencies or even suppressing them.^{13,14} Usually, these flappers are either attached to the downstream side of the bluff body¹⁰ or placed leaving a gap between itself and the bluff body.⁹ Comparative studies of similar configurations of harvesters but with attached and detached flappers showed that more power was extracted from the latter.¹⁰ A similar increase in power output due to detachment has also been made recently for a harvester with a static cylinder placed in the wake of a vibrating cylinder.¹⁵

The focus of this study is to investigate the energy extracted using a VIV based harvester comprised of a rigidly fixed bluff body cylinder and a detached flapper made up of a thin flat plate in the downstream side (Fig. 1). In particular, the effect of the gap between the flapper and the cylinder on the extracted power is investigated. The cylinder is assumed to be of length s and diameter D . The flapper is taken to be of length L , breadth $b \leq s$, and thickness h and is attached to the downstream side of the cylinder at a distance d using a rigid bar. The leading edge of the flapper is fixed to a transverse rigid bar such that the flapper behaves like a cantilever plate. The direction of upstream flow with velocity U m/s is as shown in Fig. 1. Macro-fiber composite (MFC) patches of dimensions $c \times a$ are pasted near the fixed end of the flapper on the dorsal side. The mean power, P_m , harvested from the system in duration $[t_1, t_2]$ is given by

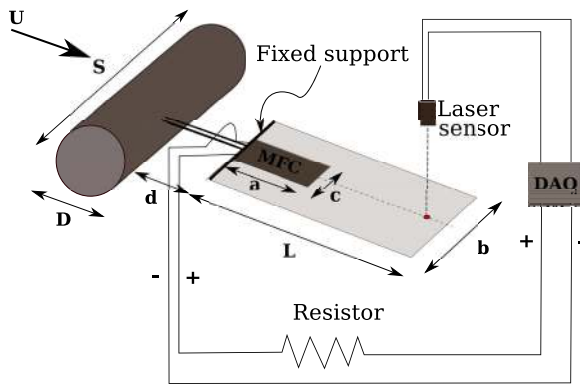


FIG. 1. Schematic diagram for the energy harvester.

$$P_m = \frac{1}{R(t_2 - t_1)} \int_{t_1}^{t_2} V^2(t) dt, \quad (1)$$

where R and $V(t)$ are the resistive load and the voltage output of the harvester at any instant of time t , respectively.

A prototype of the harvester shown in Fig. 1 is constructed for the wind tunnel experiments. The test section is 700 mm long with a cross section of 750×700 mm (Fig. 2). A steel cylinder is considered such that $D = 80$ mm and $s = 250$ mm. The flapper is made of aluminium having dimensions $L = 170$ mm, $b = 90$ mm, and $h = 0.3$ mm. The gap is taken to be $d = 2D = 160$ mm and is as per the recommendations in Refs. 10 and 16 for maximum displacements at the trailing edge of the flapper. A MFC patch of dimensions $a = 50$ mm and $c = 20$ mm was attached to the flapper by vacuum pressing, close to the leading edge and placed symmetrically about the midsection of the flapper. The wind tunnel was operated in the suction mode to ensure uniform flow conditions.

The electrical power output was measured by passing the MFC patch voltage through a resistance of $R = 300$ k Ω . Additionally, the flapper displacements were measured at a point 20 mm from the trailing edge along the midsection of the flapper, using a Wenglor opto NCDT type laser displacement sensor. The displacement and voltage measurements were

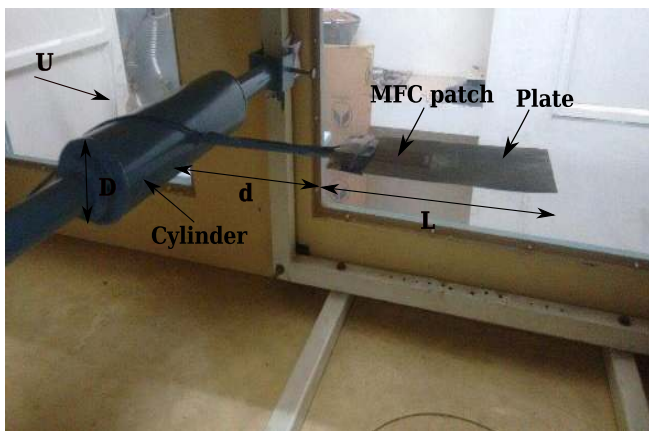


FIG. 2. Photograph of the harvester setup in the open-loop, closed section Eiffel type wind tunnel in the Biomimetics and Dynamics Laboratory of the Department of Aerospace Engineering in the Indian Institute of Technology Madras.

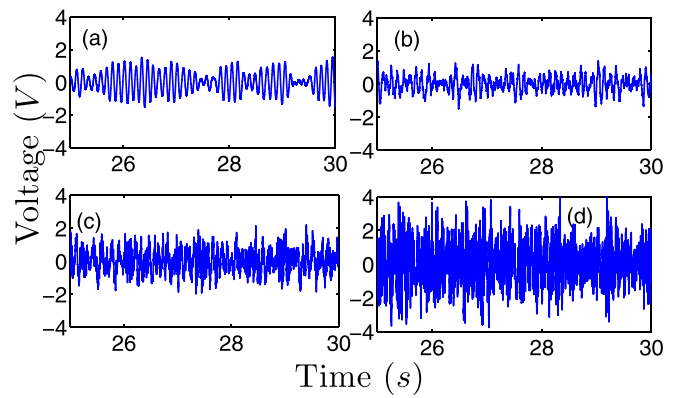


FIG. 3. MFC voltage time histories for flow velocities (a) 2.5 m/s, (b) 6.5 m/s, (c) 8.5 m/s, and (d) 10.5 m/s.

acquired through a 4-channel ATALON Data Acquisition system.

Wind tunnel tests were carried out for flow velocities 2–11 m/s, and the MFC voltage time histories were recorded (Fig. 3) for segments of time histories at different flow velocities U . The voltage signal is observed to be weak at low flow velocities and gradually gains strength with an increase in U , barring a local spike about $U = 3$ m/s. The corresponding frequency spectra shown in Fig. 4 reveal an interesting phenomenon. The frequency spectrum for MFC voltage has a single peak at 9.69 Hz for $U = 2.5$ m/s. However, for higher U , an additional frequency component emerges whose strength increases with U . As U is increased, both the peaks have a rightward shift along the frequency axis.

The mean power output P_m computed using Eq. (1) for the range of flow velocities is shown in Fig. 5(a). It is observed that the power curve can be qualitatively demarcated into three regimes. Regime 1 shows a local peak for $U = 3$ m/s. In regime 2, the extracted power varies linearly with U with a small positive slope; the magnitude of the power extracted is lower than the peak power extracted in regime 1. Regime 3 is characterized by significantly higher power extraction. An inspection of the efficiency of the power extracted in regime 3 as U varies [see Fig. 5(b)] reveals a steady increase in efficiency till $U = 10$ m/s; subsequently, even though the power extracted is higher, there is a saturation in η . Here, $\eta = P'_m/P'_{air}$, where P'_m is the power output per unit volume of the MFC. P'_{air} is the input flow power density per unit volume of the harvester¹⁷ and is

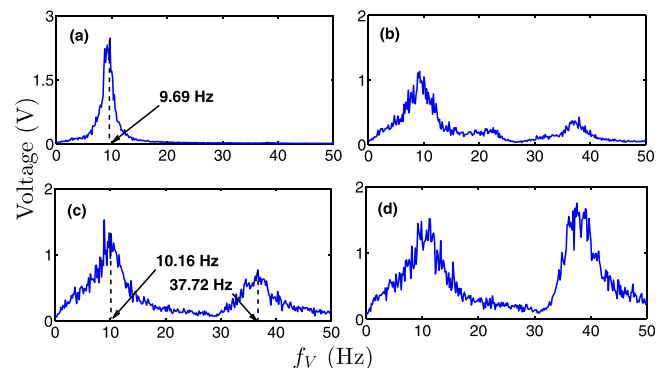


FIG. 4. Frequency spectra for the MFC voltage for flow velocities (a) 2.5 m/s, (b) 6.5 m/s, (c) 8.5 m/s, and (d) 10.5 m/s.

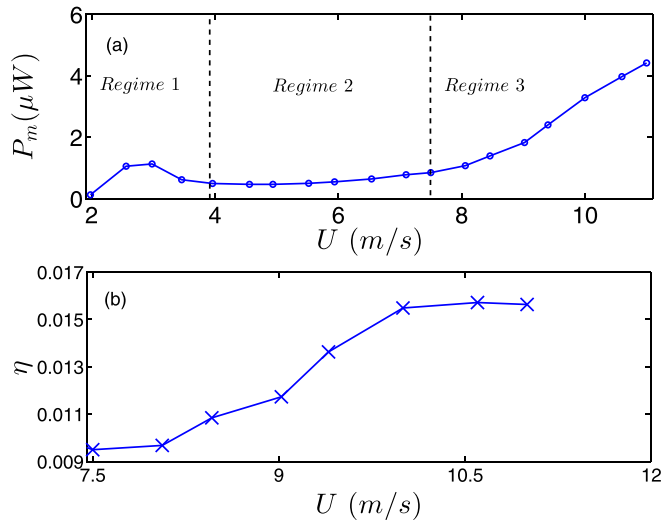


FIG. 5. (a) Variation of mean power output P_m and (b) variation of efficiency with a change in flow velocity U m/s in regime 3.

$P'_{air} = (1/2)A_f\rho U^3/(A_f(D + d + L))$, and A_f is the frontal area of the harvester.

A numerical analysis is carried out to gain an understanding about this variation in the power extracted from the harvester. The flow, the rigid bluff body, and the flexible flapper are numerically modelled taking into account the coupled dynamical interaction effects. The fluid-structure interaction (FSI) numerical framework consists of an incompressible Navier-Stokes (N-S) solver coupled with a nonlinear elastic structural model through a partitioned approach based strong coupling method.¹⁸ The N-S equation expressed in the arbitrary Lagrangian-Eulerian (ALE) formulation is solved over a time varying computational domain using a moving grid. A large strain elastic stress analysis solver based on Lagrangian displacement formulation is implemented for resolving the structure dynamics.¹⁹ The FSI solver has been tested and validated with the existing literature.^{19,20} A rectangular computational domain of length $15D$ along the longitudinal axis of the harvester and breadth $10D$ along the transverse axis is considered. The harvester is placed along the mid-axis of this domain, such that the inlet is $1D$ upstream of the cylinder. The domain dimensions are selected so that wall effects are negligible in the Computational Fluid Dynamics (CFD) computations. The domain is discretized using a structured grid; the mesh resolution has been chosen through a grid independence study.²⁰

For flow past a circular cylinder with no downstream structures disturbing its wake, vortex shedding results in a von Kármán vortex street downstream of the body. Prior to shedding, vortices are built-up when the two opposite sense shear layers emanating from either side of the cylinder interact at a distance $1D-2D$ downstream of the cylinder, in what is known as the vortex formation length (L_f). However, in the presence of a downstream structure, the shear layers separately impinge on the flapper as their interaction is obstructed. Depending on the length of the flapper, the shear layers may shed vortices downstream of the flapper or simply reattach to the flapper, forming a nearly steady recirculation bubble.^{9,13,14,16,21,22} Thus, for a given flow velocity and small values of gap d , the vortex shedding may be totally

absent or happen downstream of the flapper; for higher d , vortices are shed ahead of the flapper. Since these vortices are the driving forces for the flapper vibrations, any spatio-temporal changes in the vortices affect the flapper vibrations and, in turn, the energy harvested.

Rather than changing the gap length d for a specified U , an equivalent parametric study can be carried out by keeping d constant and increasing U . This leads to a decrease in L_f ¹⁴ and beyond a critical velocity can eventually lead to the vortices being shed between the cylinder and the flapper. For sub-critical velocities, the shedding may altogether be suppressed or happen downstream of the flapper depending on the relative numerical values of d and L .

The detailed flow field for a range of Re is investigated to understand the effect of the gap between the cylinder and the flapper in the vortex shedding. Two qualitatively distinct flow patterns are presented in terms of vorticity contours for $Re = 500$ and 1000 in Fig. 6. At $Re = 500$, the presence of the flexible flapper with a gap twice the diameter of the cylinder is seen to inhibit the shedding immediately behind the cylinder. Rather, the vortex cores deform by convecting over the flexible plate, inducing in it a moderate vibration, and subsequently sheds downstream of the flapper. The spatio-temporal impingement of the vortices on the flapper leads to a deformation of the flapper that resembles the first mode shape, causing it to vibrate in the first natural frequency. At $Re = 1000$, the vortices are observed to shed in the gap with smaller L_f , which subsequently triggers the vibration of the flapper. In other words, a natural von Kármán shedding starts taking place. Moreover, it is evident that the shedding frequency is higher than the previous cases, as indicated by the rapid change in the flow pattern with every snapshot. Besides, vortex induced vibration of the flexible plate is seen to be enhanced remarkably in terms of its higher mode shapes. The shape of the flapper seems to be governed by the number of vortices convecting along its surfaces at a given time instant which, in turn, excites higher modes.

From the flow fields presented here, it is evident that a transition in the mode of vortex shedding happens due to L_f decreasing with increasing Re . For the pre-transition case,

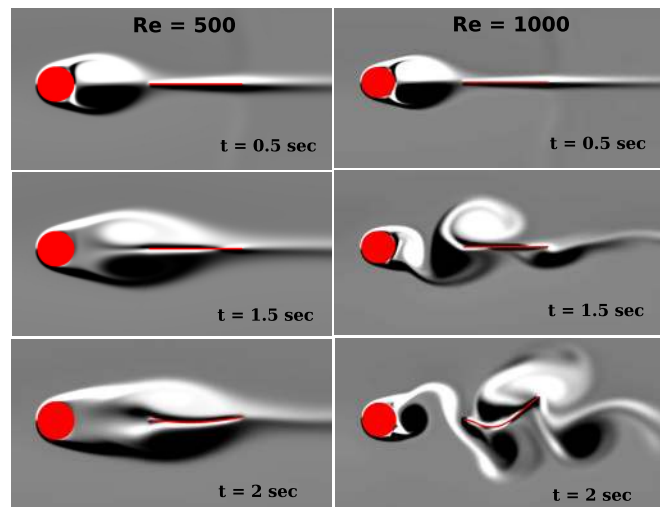


FIG. 6. Comparison of vorticity contours at $Re = 500$ and $Re = 1000$ at different time instances.

the vortex formation length could be greater than $5D$ ($D+d+L$) since the interaction between the shear layers happens only beyond the flapper. On the contrary, in the post transition regime, the formation length L_f is lower than the gap ($2D$), as L_f decreases with an increase in U . The change from an inhibited vortex shedding to a natural shedding behaviour seems to occur almost abruptly. A change in the formation length also causes a similar abrupt change in the vortex shedding frequency, denoted non-dimensionally as the Strouhal number $St = f_s L_S / U$. Here, f_s is the vortex shedding frequency and L_S is taken to be the diameter of the bluff body.

The numerical results suggest that there exist two distinct regimes of fluid flow around the flapper depending on whether vortex shedding occurs behind or ahead of the flapper. This in turn affects the flapper vibrations. Figure 7 shows the variation of peak amplitude and the root mean square (rms) displacement of the flapper at a location near the trailing edge along the midsection. These observations are qualitatively consistent with the reported literature.⁹ The local peak at $U = 3$ m/s can be attributed to a lock in of the shedding frequency with the first natural frequency of the flapper.¹⁶

The frequency spectra of the flapper displacements for various U are investigated. The frequency of the flapper oscillations can be represented in terms of a non-dimensional number $St_p = f_p L_S / U$, where f_p is the dominant frequency obtained from the displacement frequency spectra at a particular U and L_S is the length scale associated with the system, which can be taken to be equal to L_f . This implies that $L_S = D$ when vortex shedding occurs ahead of the flapper and $L_S = L + d + D$ when shedding occurs behind the flapper. When $L_S = D$, the St_p values undergo a jump at $U = 7.5$ m/s; these values are close to 0.2 which is the Strouhal number typically considered for the Reynolds number for the range of flows considered in this study.¹² This suggests that St_p and St are closely related and indirectly confirm that the plate oscillates at the frequencies of vortex shedding, and the flapper oscillations are indeed due to the forcing generated by

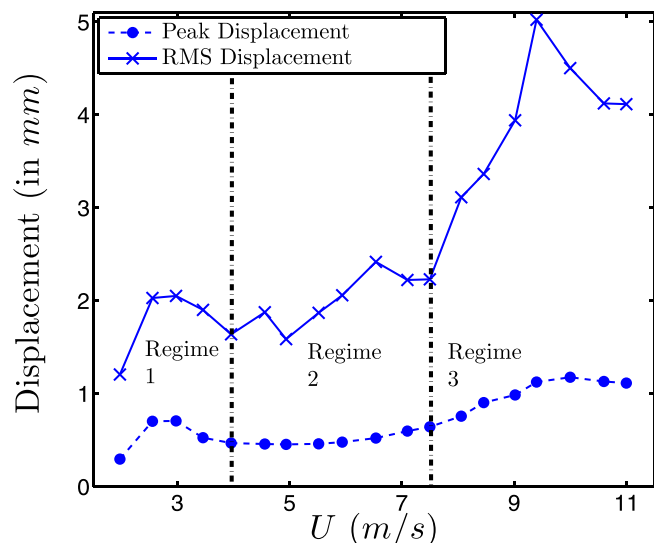


FIG. 7. Peak and RMS deviation of the flapper response for different flow velocities.

cylinder wake vortices. A similar jump in St_p can be observed when $L_S = L + d + D$ (see Fig. 8) although the values are much higher. However, using $L_S = L + d + D$ for regime 2 and $L_S = D$ for regime 3, it is observed that the variation of St_p with U is without any significant jumps. This trend is similar to the formation length based Strouhal number reported in the literature.¹⁴ These observations are significant as the convention in the energy harvesting community is to consider a constant Strouhal number, typically taken to be 0.2.

It is pertinent to note that despite the jump in f_p as U is varied, the mean power curve shown in Fig. 5 does not exhibit any sharp jump. The relatively smooth trend is similar to that of the rms displacements of the flapper (see Fig. 7). However, it can be seen that a marked rise in rms displacements, as well as in P_m , is observed only in the vicinity of $U = 7.5$ m/s where there is a jump in St_p . In regime 3, the vortices are well developed and impinge larger forces on the flapper, resulting in more vigorous vibrations. On the other hand, in regime 2, the vortices either occur beyond the trailing edge of the flapper or are not well developed over the flapper resulting in weaker vibrations. This explains the higher power extracted in regime 3, where $U > 7.5$ m/s.

Figure 5 shows that the power efficiency does not increase beyond a specified flow speed. It can be hypothesized that at these higher values of U , the vortex shedding frequency is large enough so that more than two vortices impinge on the flapper at each time instant. This implies that the spatio-temporal deflection of the flapper induces higher modes to be excited. As the placement of the MFC patches is optimal only for efficient harvesting of energy when the flapper vibrates in the first mode, the power extraction is inefficient at flow speeds higher than $U = 9.8$ m/s. More studies need to be carried out to investigate this further.

It is a common trend in flow energy harvester community to assume that an energy harvester would oscillate in its first modeshape.¹⁷ From the results presented here, it is evident that the change in the regime of vortex shedding is accompanied by a change in the dominant mode shape, leading to a sub-optimal power extraction despite stronger fluid forces. The efficiency of power extracted is observed to be

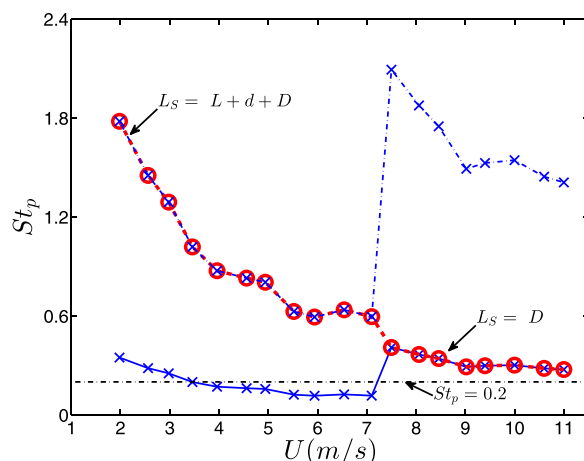


FIG. 8. Non-dimensional frequency of flapper oscillations for different flow velocities with two length scales, D and $L + d + D$. The dotted line shows a more realistic St_p with different L_S in different regimes.

higher when the formation length is smaller than the gap, and the vortices are well developed ahead of the leading edge of the flapper. Thus, while designing a flapper to resonate with vortex shedding frequency at a particular flow velocity, the variability in St due to the presence of the flapper must be taken into account. These observations imply that in addition to the flapper stiffness, the gap should also be optimal to permit resonant oscillations at a design flow velocity. The presence of two different frequencies, and the possible dependence on the plate length and gap, provides additional control parameters in the design of the harvester. For instance, it could be possible to choose d and L such that the two shedding frequencies correspond to two natural frequencies of the flapper. Thus, the phenomenon of frequency jump poses both challenges and opportunities in the energy harvester design. This behaviour has escaped the attention of researchers since the configurations studied in the literature typically had a narrow gap between the cylinder and the flapper.

¹A. Abdelkefi, *Int. J. Eng. Sci.* **100**, 112 (2016).

²D. Li, Y. Wu, A. Ronch, and J. Xiang, *Prog. Aerosp. Sci.* **86**, 28 (2016).

³E. Naudascher and D. Rockwell, *Flow-Induced Vibrations: An Engineering Guide* (Courier Corporation, 2012).

⁴Z. Peng and Q. Zhu, *Phys. Fluids* **21**, 123602 (2009).

⁵Q. Zhu and Z. Peng, *Phys. Fluids* **21**, 033601 (2009).

⁶J. McCarthy, S. Watkins, A. Deivasigamani, and S. John, *J. Sound Vib.* **361**, 355 (2016).

⁷J. Young, J. C. Lai, and M. F. Platzer, *Prog. Aerosp. Sci.* **67**, 2 (2014).

⁸Q. Xiao and Q. Zhu, *J. Fluids Struct.* **46**, 174 (2014).

⁹J. Allen and A. Smits, *J. Fluids Struct.* **15**, 629 (2001).

¹⁰H. Akaydin, N. Elvin, and Y. Andreopoulos, *Exp. Fluids* **49**, 291 (2010).

¹¹S. Shi, T. New, and Y. Liu, *Exp. Therm. Fluid Sci.* **46**, 151 (2013).

¹²R. D. Blevins, *Flow-Induced Vibration* (Van Nostrand Reinhold Co., Inc., New York, NY, USA, 1990).

¹³A. Roshko, "On the drag and shedding frequency of two-dimensional bluff bodies," Technical Report No. NACA-TN-3169, DTIC Document, 1954.

¹⁴J. Gerrard, *J. Fluid Mech.* **25**, 401 (1966).

¹⁵L. Zhang, H. Dai, A. Abdelkefi, and L. Wang, *Appl. Phys. Lett.* **111**, 073904 (2017).

¹⁶Y. Lau, R. So, and R. Leung, *J. Fluids Struct.* **19**, 1061 (2004).

¹⁷H. Akaydin, N. Elvin, and Y. Andreopoulos, *Smart Mater. Struct.* **21**, 025007 (2012).

¹⁸C. Michler, S. Hulshoff, E. Van Brummelen, and R. De Borst, *Comput. Fluids* **33**, 839 (2004).

¹⁹Z. Tukovic, P. Cardiff, A. Karac, H. Jasak, and A. Ivankovic, in 9th OpenFOAM Workshop, Zagreb, Croatia (2014).

²⁰C. Bose, S. K. Kumar, S. Sarkar, and S. Gupta, in Proceedings of the Structural Engineering Convention, 2016.

²¹M. Unal and D. Rockwell, *J. Fluid Mech.* **190**, 491 (1988).

²²Y. Nakamura, *J. Fluids Struct.* **10**, 147 (1996).